SCIENCE CHINA
Chemistry

• ARTICLES •

HOT PAPERS

February 2017 Vol.60 No.2:257–263
doi: 10.1007/s11426-016-0336-6

Rhodanine flanked indacenodithiophene as non-fullerene acceptor for efficient polymer solar cells

Boyu Jia[1], Yao Wu[1], Fuwen Zhao[2], Cenqi Yan[1], Siya Zhu[1], Pei Cheng[2], Jiangquan Mai[3], Tsz-Ki Lau[3], Xinhui Lu[3], Chun-Jen Su[4], Chunru Wang[2] & Xiaowei Zhan[1*]

[1]*Key Laboratory of Polymer Chemistry and Physics of Ministry of Education, Department of Materials Science and Engineering, College of Engineering, Peking University, Beijing 100871, China*
[2]*Institute of Chemistry, Chinese Academy of Sciences, Beijing 100190, China*
[3]*Department of Physics, Chinese University of Hong Kong, New Territories, Hong Kong, China*
[4]*National Synchrotron Radiation Research Center, Taiwan 30076, China*

Received August 14, 2016; accepted September 27, 2016; published online January 3, 2017

A fused-ring electron acceptor IDT-2BR1 based on indacenodithiophene core with hexyl side-chains flanked by benzothiadiazole rhodanine was designed and synthesized. In comparison with its counterpart with hexylphenyl side-chains (IDT-2BR), IDT-2BR1 exhibits higher highest occupied molecular orbital (HOMO) energy but similar lowest unoccupied molecular orbital (LUMO) energy (IDT-2BR1: HOMO=−5.37eV, LUMO=−3.67eV; IDT-2BR: HOMO=−5.52eV, LUMO=−3.69eV), red-shifted absorption and narrower bandgap. IDT-2BR1 has higher electron mobility (2.2×10^{-3} cm^2 V^{-1} s^{-1}) than IDT-2BR (3.4×10^{-4} cm^2 V^{-1} s^{-1}) due to the reduced steric hindrance and ordered molecular packing. Fullerene-free organic solar cells based on PTB7-Th:IDT-2BR1 yield power conversion efficiencies up to 8.7%, higher than that of PTB7-Th:IDT-2BR (7.7%), with a high open circuit voltage of 0.95 V and good device stability.

organic solar cell, non-fullerene acceptor, fused-ring electron acceptor, indacenodithiophene, rhodanine

Citation: Jia B, Wu Y, Zhao F, Yan C, Zhu S, Cheng P, Mai J, Lau TK, Lu X, Su CJ, Wang C, Zhan X. Rhodanine flanked indacenodithiophene as non-fullerene acceptor for efficient polymer solar cells . *Sci China Chem*, 2017, 60: 257–263, doi: 10.1007/s11426-016-0336-6

1 Introduction

As fossil fuel production and use give rise to environmental pollution, and their storage is diminishing, human beings have paid great attention to clean energy, such as solar cells. Bulk heterojunction (BHJ) organic solar cells (OSCs) have attracted much attention due to some advantages, such as low cost, light weight, flexibility and large area fabrication [1–3]. Fullerenes and their derivatives, such as $PC_{61}BM$ and $PC_{71}BM$, are dominated electron acceptors in OSCs [4]. However, to overcome innate drawbacks of fullerenes, such as weak absorption in the visible spectral region and limited energy level variability, it is necessary to develop non-fullerene electron acceptors [5]. Recently fullerene-free OSCs have been developing at an amazing speed, and some non-fullerene OSCs have exhibited power conversion efficiencies (PCEs) of >7%, which are even higher than those of the fullerene-based control devices in some cases [6–18].

Many non-fullerene electron acceptors were designed based on 2D or quasi-2D π-conjugated systems, such as halogenated subphthalocyanine and imide/diimide-functionalized rylenes [19–27]. We reported the first electron acceptors based on indacenodithiophene (IDT) and indacenodithieno[3,2-b]thiophene (IDTT) decorated with electron-withdrawing groups [6,8,28–34]. The rigid extended fused-ring structure of IDT and IDTT can prevent the

*Corresponding author (email: xwzhan@pku.edu.cn)

© Science China Press and Springer-Verlag Berlin Heidelberg 2017

molecular skeleton from torsion and conformational change, and enhance charge carrier mobility. The energy levels and absorption of the molecules can be easily tuned by changing the end-capping groups with different electron-withdrawing units. The four peripheral substituents of the flat backbone ensure solution processability, reduce intermolecular interactions and prevent the acceptor from strong self-aggregation and large phase separation in blended films, and their solubility, crystallinity and film morphology can be tailored by changing the nature of the substituents.

In our previous work, we reported a non-fullerene acceptor IDT-2BR (Figure 1) based on IDT with four hexylphenyl side-chains; OSCs based on blend of IDT-2BR and poly(3-hexylthiophene) (P3HT) exhibited a PCE of 5.12%, higher than that of $PC_{61}BM$-based control device [31]. Structure optimization of IDT-2BR is expected to red-shift the absorption spectrum and to enhance electron transport. Generally, side-chains can affect molecular packing, absorption spectrum and charge mobility. Moreover, side-chains exert somewhat electronic effects (e.g., σ-induction, π-conjugation) and affect energy levels. Relative to 4-hexylphenyl, hexyl causes the reduced steric hindrance and stronger molecular packing. Therefore, we used hexyl side-chains to replace 4-hexylphenyl side-chains in IDT-2BR and synthesized IDT-2BR1 (Figure 1). IDT-2BR1 exhibits red-shifted absorption and higher electron mobility, which are mainly attributed to the reduced steric hindrance and stronger molecular packing. Finally, OSCs based on PTB7-Th:IDT-2BR1 yields a higher PCE of 8.7% than PTB7-Th:IDT-2BR (7.7%). OSCs based on PTB7-Th:IDT-2BR1 exhibit better thermal stability and photo stability than the $PC_{71}BM$-based control devices.

2 Experimental

2.1 Synthesis

2.1.1 Synthesis of compound **3**

To a three-necked round-bottomed flask were added compound **1** (464 mg, 0.50 mmol), compound **2** (243 mg, 1.0 mmol), and toluene (30 mL). The mixture was deoxygenated with nitrogen for 15 min, and then $Pd(PPh_3)_4$ (30 mg, 0.026 mmol) was added. The mixture was refluxed for 48 h and then cooled to room temperature. 100 mL of water was added and the mixture was extracted with $CHCl_3$ (2×100 mL). The organic phase was dried over anhydrous $MgSO_4$. After removing the solvent, the residue was purified by column chromatography on silica gel using petroleum ether/$CHCl_3$ (1:2) as eluent yielding a purple solid (362 mg, 78%). ^{1}H NMR (400 MHz, CD_2Cl_2): δ (ppm) 10.72 (s, 2H), 8.31 (s, 2H), 8.25 (d, J=7.8 Hz, 2H), 8.09 (d, J=7.8 Hz, 2H), 7.52 (s, 2H), 2.20 (m, 8H), 1.14 (m, 24H), 0.98 (m, 8H), 0.78 (t, J=6.8Hz, 12H). ^{13}C NMR (100 MHz, $CDCl_3$): δ (ppm) 188.5, 157.0, 154.3, 154.0, 152.3, 147.0, 140.7, 136.4, 134.1, 133.0, 124.8, 122.8, 114.1, 54.4, 39.2, 31.6, 29.7, 24.3, 22.6, 14.0. MS (MALDI): m/z 926 (M^+). Anal. calc. for $C_{54}H_{62}N_4O_2S_4$: C, 69.94%; H, 6.74%; N, 6.04%. Found: C, 70.03%; H, 6.80%; N, 6.01%.

2.1.2 Synthesis of IDT-2BR1

To a three-necked round-bottomed flask were added compound **3** (148 mg, 0.16 mmol), 3-ethylrhodanine (258 mg, 1.6 mmol), chloroform (30 mL), and triethylamine (0.5 mL). The mixture was deoxygenated with nitrogen for 15 min and then refluxed for 12 h. After cooling to room temperature, the mixture was poured into methanol (300 mL) and filtered. The residue was purified by column chromatography on silica gel using petroleum ether/$CHCl_3$ (1:2) as eluent yielding a dark green solid (150 mg, 77%). ^{1}H NMR (400 MHz, $CDCl_3$): δ (ppm) 8.59 (s, 2H), 8.27 (s, 2H), 8.08 (d, J=7.8 Hz, 2H), 7.80 (d, J=7.8 Hz, 2H), 7.49 (s, 2H), 4.34 (m, 4H), 2.22 (m, 8H), 1.41 (t, J=7.2, 8H), 1.32 (s, 6H), 1.21 (m, 24H), 0.84 (t, J=6.8 Hz, 12H). ^{13}C NMR (100 MHz, $CDCl_3$): δ (ppm) 192.0, 166.6, 156.0, 153.6, 153.2, 150.8, 145.1, 140.0, 135.4, 130.3, 129.6, 126.3, 123.5, 123.3, 123.0, 122.8, 112.9, 53.4, 38.9, 38.2, 30.6, 28.7, 23.2, 21.5, 13.0, 11.3. MS (MALDI): m/z 1212 (M^+). Anal. calc. for $C_{64}H_{72}N_6O_2S_8$: C, 63.33%; H, 5.98%; N, 6.92%. Found: C, 63.40%; H, 6.00%; N, 6.89%.

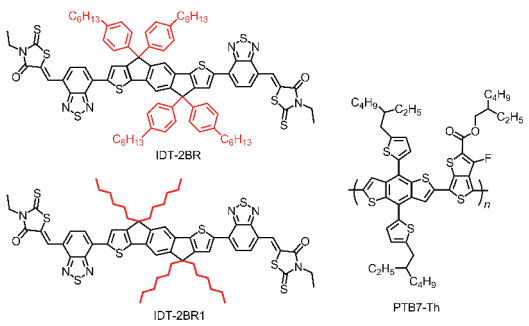

Figure 1 Chemical structures of IDT-2BR, IDT-2BR1 and PTB7-Th (color online).

2.2 Fabrication and characterization of photovoltaic cells

OSCs were fabricated with the structure of ITO/PEDOT:PSS/PTB7-Th:IDT-2BR or IDT-2BR1/Ca/Al. The patterned indium tin oxide (ITO) glass (sheet resistance=15 Ω $\square^{-1}$) was pre-cleaned in an ultrasonic bath of acetone and isopropanol, and treated in an ultraviolet-ozone chamber (Jelight Company, USA) for 20 min. A thin layer (35 nm) of poly(3,4-ethylenedioxythiophene):poly(styrene sulfonate) (PEDOT:PSS, Baytron PVP AI 4083, Germany) was spin-coated onto the ITO glass and baked at 150 °C for 20 min. PTB7-Th:IDT-2BR or IDT-2BR1 mixture (15 mg mL^{-1} in total) in *o*-dichlorobenzene (*o*-DCB) and chloroform

(CF) (4:1, *v*/*v*) with 3% 1-chloronaphthalene (CN), was spin-coated on the PEDOT:PSS layer to form a photosensitive layer (ca. 80 nm). The thickness of photosensitive layer was measured using a Bruker DektakXT profilometer (Germany). The calcium layer (ca. 20 nm) and the aluminum layer (ca. 100 nm) were then evaporated onto the surface of the photosensitive layer under vacuum (ca. 10^{-5} Pa) to form the negative electrode. The active area of the device was measured using optical microscope without an aperture and was ca. 4 mm^2.

Inverted OSCs were fabricated with a structure of ITO/ZnO/PTB7-Th:IDT-2BR or IDT-2BR1/MoO_x/Ag. Patterned ITO glass (sheet resistance=15Ω $\square^{-1}$) was pre-cleaned in an ultrasonic bath with acetone and isopropanol, and treated in an ultraviolet ozone chamber (Jelight Company, USA) for 20 min. ZnO electron transport layers were prepared onto the ITO glass through spin coating at 3000 r min^{-1} from a ZnO precursor solution. Then ZnO substrates were immediately baked in air at 200 °C for 30 min. An *o*-DCB/CF solution (4:1, *v*/*v*) (totally 15 mg mL^{-1}) of PTB7-Th:IDT-2BR1 or IDT-2BR blend was subsequently spin-coated (1000 r min^{-1}) on the ZnO layer to form a photosensitive layer (ca. 80 nm). Thin layer (5 nm) of MoO_3 was deposited as the anode interlayer, and 80 nm of Ag was deposited as the top electrode. The active area of the device was ca. 4 mm^2.

The density-voltage (*J*-*V*) curve was measured using a computer-controlled B2912A precision source/measure unit (Agilent Technologies, USA). An XES-70S1 (SAN-EI Electric Co., Ltd., Japan) solar simulator (AAA grade, 70 mm×70 mm photobeam size) coupled with AM 1.5 G solar spectrum filters was used as the light source, and the optical power at the sample was 100 mW cm^{-2}. A 2 cm×2 cm monocrystalline silicon reference cell (SRC-1000-TC-QZ) was purchased from VLSI Standards Inc. (USA). The incident photons to converted current efficiency (IPCE) spectrum was measured using a solar cell spectral response measurement system QE-R3011 (Enlitech Co., Ltd., Taiwan, China). The light intensity at each wavelength was calibrated using a standard single crystal Si photovoltaic cell.

3 Results and discussion

3.1 Theoretical calculation of molecular configuration

We carried out density function theoretical calculation to analyse the molecular configuration of IDT-2BR1 using the Gaussian 09 program (Figure 2). The molecular backbone of IDT-2BR1 adopts a nearly flat configuration with four non-planar hexyl chains, which are almost perpendicular to the backbone. The coplanar backbone configuration is beneficial to π-π stacking and charge transport. Four non-planar substituents can weaken intermolecular interaction and refrain from severe aggregation and large-scale phase separation. In comparison with IDT-2BR [31], whose side chains exhibit a dihedral angle of ca. 115° to the backbone plane, IDT-2BR1 possesses more perfect configuration, which leads to more ordered aggregation to attain an enhanced electron mobility.

3.2 Molecular synthesis and characterization

The compound IDT-2BR1 was synthesized by two facile reactions (Scheme 1). The new intermediate **3** was synthesized through Stille coupling reaction of two commercial available reagents **1** and **2** using $Pd(PPh_3)_4$ as the catalyst in a 78% yield. Subsequent Knoevenagel condensation between compound **3** and 3-ethylrhodanine afforded IDT-2BR1 in a 77% yield. Compounds **3** and IDT-2BR1 were fully characterized by matrix-assisted laser desorption ionization-time of flight mass spectrometry (MALDI-TOF MS), ^{1}H NMR, ^{13}C NMR, and elemental analysis. The thermal property of IDT-2BR1 was investigated by thermo gravimetric analysis (TGA). The compound exhibits excellent thermal stability with a decomposition temperature (5% weight loss) of 377 °C in nitrogen atmosphere (Figure S1, Supporting Information online).

The normalized spectra of optical absorption of IDT-2BR1 and IDT-2BR in chloroform solution (10^{-6} M) and in solid film are shown in Figure S1(b) and Figure 3(a), respectively. The IDT-2BR1 solution exhibits broad and strong absorption in 500−760 nm region with a maximum extinction coefficient of 1.5×10^5 M^{-1} cm^{-1} at 650 nm. Compared with the solution, IDT-2BR1 film shows a 40 nm red-shifted peak with a strong shoulder peak, indicating that self-organization behavior exists in film. The absorption peak of IDT-2BR1 film red-shifts 32 nm is relative to that of IDT-2BR film. The optical band-

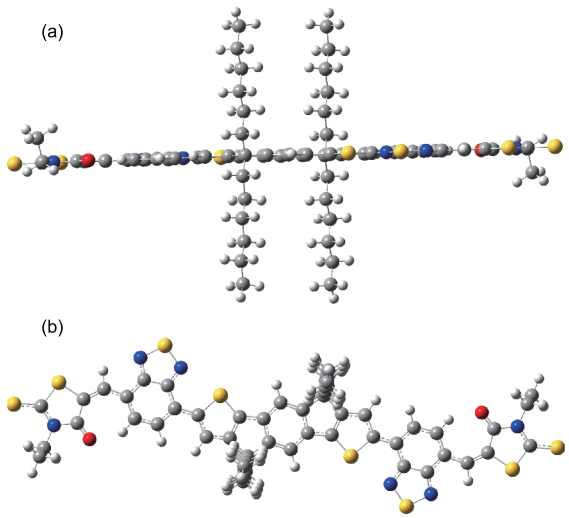

Figure 2 Optimized geometries of IDT-2BR1. (a) Side view; (b) top view (color online).

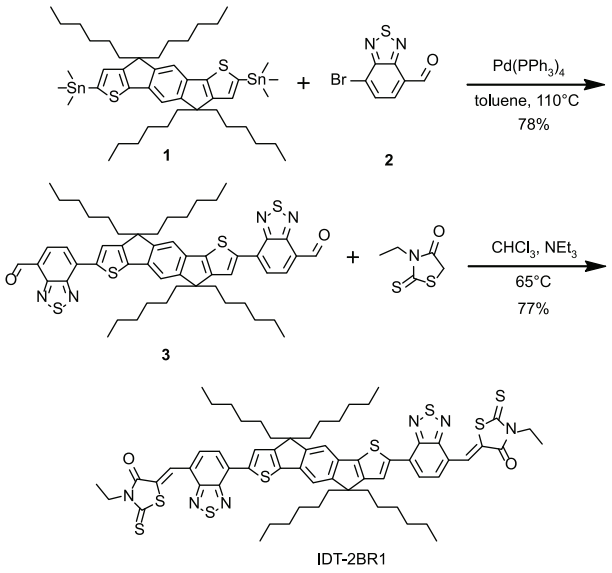

Scheme 1 Synthesis of IDT-2BR1.

gap of IDT-2BR1 estimated from the absorption edge of the thin film (764 nm) is 1.61 eV, narrower than that of IDT-2BR (1.68 eV). The higher highest occupied molecular orbital (HOMO) and lowest unoccupied molecular orbital (LUMO) energies of IDT-2BR1 film are estimated to be –5.37 and –3.67 eV from the onset oxidation and reduction potentials from electrochemical cyclic voltammetry (Figure 3(b)). IDT-2BR1 shows higher HOMO but similar LUMO relative to IDT-2BR (HOMO=–5.52 eV, LUMO=–3.69 eV).

3.3 Photovoltaic properties

To demonstrate potential application of IDT-2BR1 in OSCs, we selected PTB7-Th [35] as a donor and IDT-2BR1 or IDT-2BR as an acceptor to fabricate BHJ devices with a structure of ITO/PEDOT:PSS/PTB7-Th:IDT-2BR1 or IDT-2BR/Ca/Al. Table S1 (Supporting Information online) summarizes open circuit voltage (V_{OC}), short circuit current density (J_{SC}), fill factor (FF), and PCE of the devices with different donor/acceptor (D/A) weight ratios and different processing solvents. These devices yield very high V_{OC} of ca. 1 V due to the large difference between LUMO of IDT-2BR1 and HOMO of PTB7-Th (1.53 eV). The devices based on D/A weight ratio of 1:1 perform best (Figure S2(a)). Since IDT-2BR1 has limited solubility in *o*-DCB and good solubility in CF, we used mixed solvent of 80% *o*-DCB/20% CF to improve quality of PTB7-Th:IDT-2BR1 blended film; the mixed solvent increases J_{SC} of OSCs relative to *o*-DCB (Figure S2(b)). Furthermore, adding 3% CN additive in the mixed solvent enhances PCE of the OSCs based on PTB7-Th:IDT-2BR1 blend to 7.4%, which is higher than that of PTB7-Th:IDT-2BR blend (6.3%) (Figure S3).

The inverted OSCs based on PTB7-Th:IDT-2BR1 blend exhibit even higher PCE of up to 8.7%, which is higher than that of PTB7-Th:IDT-2BR blend (7.7%) (Figure 4(a), Table 1). Figure 4(b) shows the IPCE curve of the inverted devices based on PTB7-Th:IDT-2BR1. The IPCE spectrum of the device covers a broad response of 300–800 nm. The J_{SC} calculated from integration of the IPCE spectrum with the AM 1.5G reference spectrum is 14.5 mA cm^{-2}, which is similar to that obtained from *J*-*V* measurement (the error is 4.6%).

We investigated the stability of the OSCs based on PTB7-Th:IDT-2BR1 and PTB7-Th:IDT-2BR and compared with that of PTB7-Th:$PC_{71}BM$ (Figure S4). After heating at 100 °C for 3 h, the PCE of the OSCs based on PTB7-Th:IDT-2BR1 and PTB7-Th:IDT-2BR kept 83% of original value, while that of PTB7-Th:$PC_{71}BM$ kept 62% of original value, indicating that the non-fullerene OSCs exhibit better thermal stability than the fullerene OSCs (Figure S4(a)). The OSCs based on PTB7-Th:IDT-2BR1 and PTB7-Th:IDT-2BR also exhibit better photo stability than the $PC_{71}BM$-based OSCs under continuous illumination of AM 1.5G, 100 mW cm^{-2} (Figure S4(b)).

Electron mobility of IDT-2BR1 pristine film and electron and hole mobilities of PTB7-Th:IDT-2BR1 blended films were measured by space-charge limited current (SCLC) method with the device structure of ITO/PEDOT:PSS/active

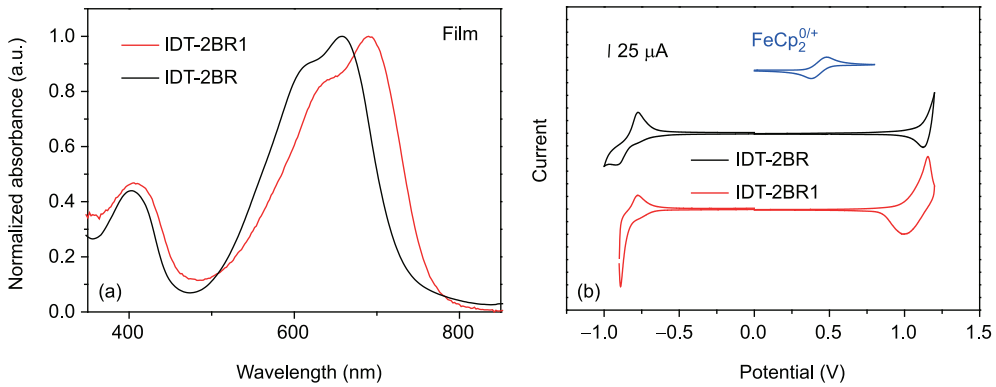

Figure 3 (a) Absorption spectra of IDT-2BR1 and IDT-2BR in film; (b) cyclic voltammograms for IDT-2BR1 and IDT-2BR in CH_3CN/0.1 M Bu_4NPF_6 at 100 mV s^{-1}, the horizontal scale refers to an Ag/AgCl electrode as a reference electrode (color online).

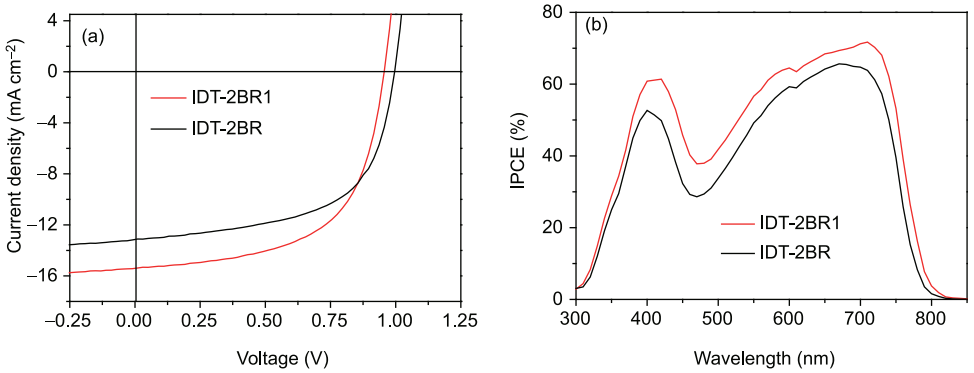

Figure 4 (a) The *J-V* curves and (b) IPCE curves of inverted devices based on PTB7-Th:IDT-2BR1 or IDT-2BR (1:1, *w*/*w*) under the illumination of AM 1.5 G, 100 mW cm^{-2} (color online).

Table 1 Photovoltaic performance of the OSCs based on PTB7-Th:IDT-2BR or IDT-2BR1

Acceptor	CF (%)	CN (%)	V_{OC} (V)	J_{SC} (mA cm^{-2})	FF (%)	PCE (%)	
						Best	Ave. [a]
IDT-2BR1	20	3	0.95	15.2	60.0	8.7	8.6
IDT-2BR	20	3	0.99	13.0	60.0	7.7	7.6

a) The average PCE is obtained from over 15 devices.

layer/Au for holes and Al/active layer/Al for electrons (Figure S5), and the data are summarized in Table S2. IDT-2BR1 pristine film exhibits a relatively high electron mobility of 2.2×10^{-3} cm^2 V^{-1} s^{-1}, which is one order of magnitude higher than that of IDT-2BR (3.4×10^{-4} cm^2 V^{-1} s^{-1}) [31]. The blended film of PTB7-Th:IDT-2BR1 exhibits hole mobility of 1.5×10^{-4} cm^2 V^{-1} s^{-1} and electron mobility of 3.9×10^{-4} cm^2 V^{-1} s^{-1} with balanced hole and electron transport, which is responsible for the high FF and J_{SC}.

3.4 Film morphology

We investigated the surface morphology of PTB7-Th:IDT-2BR1 and PTB7-Th:IDT-2BR blended films by atomic force microscopy (AFM) (Figure S6(a, b)). The blended film of PTB7-Th:IDT-2BR1 exhibits relatively rougher surface with root-mean-square (RMS) roughness of 4.1 nm than PTB7-Th:IDT-2BR with RMS roughness of 3.5 nm. Transmission electron microscopy (TEM) was used to investigate the internal morphology of the active layer (Figure S6(c, d)). PTB7-Th:IDT-2BR1 exhibits clearer aggregation domains and interpenetrating network, due to enhanced crystallinity of IDT-2BR1.

The molecular packing in IDT-2BR1 neat film as well as PTB7-Th:IDT-2BR1 and PTB7-Th:IDT-2BR blended films was investigated with grazing incidence wide-angle X-ray scattering (GIWAXS) measurements [36,37]. The two-dimensional GIWAXS patterns are presented in Figure 5(a–c). Remarkably, the neat IDT-2BR1 film (Figure 5(a)) exhibits absolute "face-on" orientation with lamellar peak located along q_r axis (q_r=0.37 Å^{-1}, d=16.98 Å) and π-π stacking peak located along q_z axis (q_z=1.73 Å^{-1}, d=3.63 Å), in contrast to IDT-2BR neat film, which shows much less orientational order [31]. This is another evidence of the self-organization in IDT-2BR1 film, consistent with UV absorption results. This might be closely related to the nearly flat backbone and perpendicular hexyl chains of IDT-2BR1 indicated by our DFT calculation. The corresponding intensity integral profiles along q_z and q_r axis are presented in Figure 5(d, e). Stronger "face-on" packing order in PTB7-Th:IDT-2BR1 blended film was observed as indicated by the more intense π-π peak located along q_z axis (q_z=1.65 Å^{-1}, d=3.81 Å) (Figure 5(b)) in comparison with PTB7-Th:IDT-2BR blended film (Figure 5(c)), which is known to be beneficial to vertical charge transport.

Grazing-incidence small-angle X-ray scattering (GISAXS) was also measured to understand the nanoscale phase separation in the bulk films [38,39]. Much stronger scattering intensity was observed in IDT-2BR1 pristine film, compared with IDT-2BR pristine film, in support of the self-aggregation behavior observed in UV absorption and GIWAXS for IDT-2BR1 (Figure S7). This is reasonably accompanied with a relatively stronger phase separation in PTB7-Th:IDT-2BR1 blended film, as indicated from the appearance of the additional scattering intensity around q=0.01 Å^{-1} observed in Figure 6. By fitting the intensity profiles with models adopted by Liao *et al.* [38], we can obtain the sizes of the estimated amorphous domain and the aggregated polymer crystalline domain. The amorphous domain size is about the same (~43 nm) for both blended films. The size of aggregated polymer crystalline domain of PTB7-Th:IDT-2BR1 blended film (~21 nm) is much larger than that of PTB7-Th:IDT-2BR blended

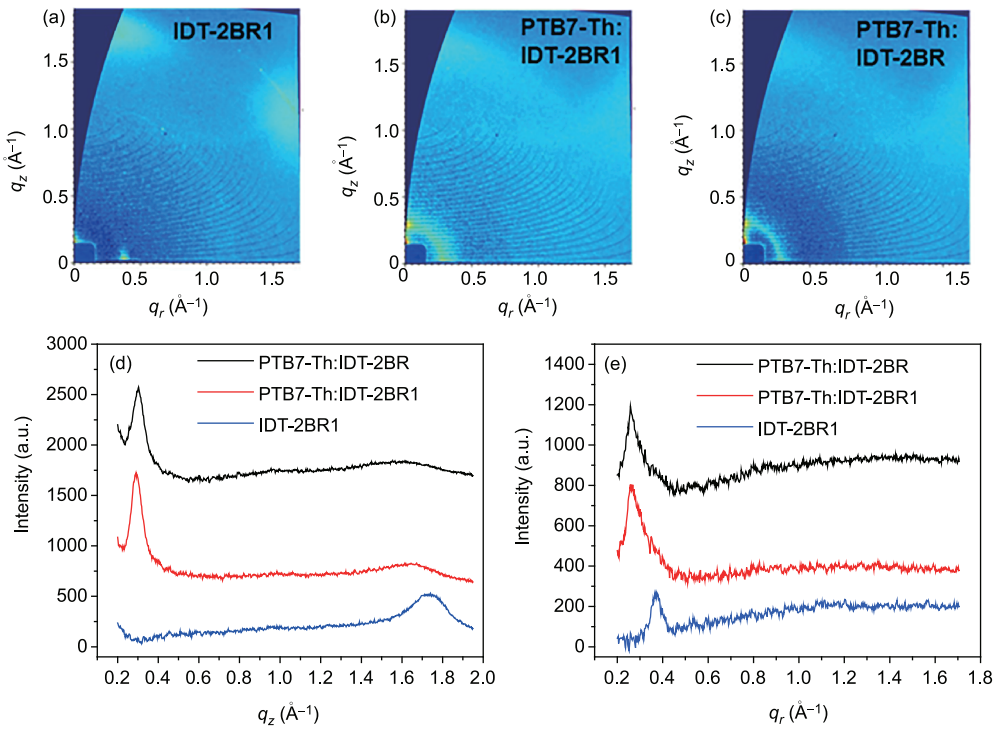

Figure 5 (a–c) 2D GIWAXS patterns of neat IDT-2BR1, PTB7-Th:IDT-2BR1 and PTB7-Th:IDT-2BR films; (d, e) the corresponding intensity profiles along q_z and q_r directions. The curves are displaced for clarity (color online).

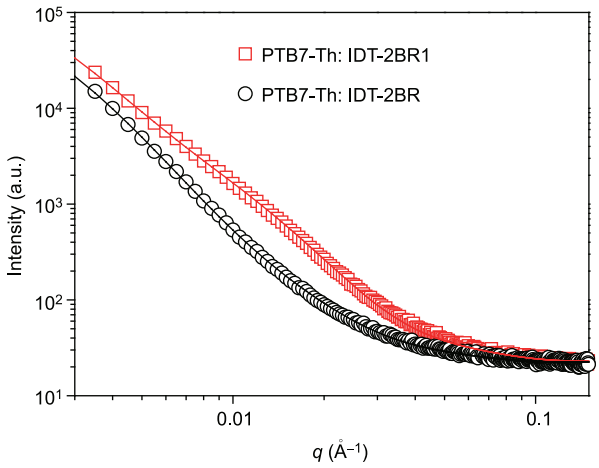

Figure 6 GISAXS intensity integral along q_z direction for PTB7-Th:IDT-2BR1 and PTB7-Th:IDT-2BR films (color online).

film (~13 nm), correlated with relatively larger electron mobility of the former. In addition, both sizes are comparable to theoretical exciton diffusion length, allowing for efficient exciton dissociation.

4 Conclusions

We designed and synthesized molecule IDT-2BR1 based on indacenodithieno[3,2-b]core. Theoretical calculations suggest that the molecular backbone adopts a nearly flat configuration with four non-planar alkyl chains. IDT-2BR1 with *n*-hexyl chains exhibits narrower bandgap, higher HOMO and higher electron mobility than its counterpart with 4-(*n*-hexyl)phenyl chains, IDT-2BR, due to the reduced steric hindrance and stronger molecular packing. Inverted OSCs based on PTB7-Th:IDT-2BR1 yield a higher PCE of 8.7% than those of PTB7-Th:IDT-2BR (7.7%). OSCs based on PTB7-Th:IDT-2BR1 exhibit better thermal stability and photo stability than the PC71BM-based control devices.

Acknowledgments This work was supported by the National Basic Research Program of China (2013CB834702), the National Natural Science Foundation of China (91433114). The supercomputing center of Chinese Academy of Sciences is acknowledged for molecular modeling. J. Mai, T. Lau and X. Lu acknowledge the financial support from Research Grant Council of Hong Kong (General Research Fund No. 14303314 and Theme-based Research Scheme No. T23-407/13-N).

Conflict of interest The authors declare that they have no conflict of interest.

Supporting information The supporting information is available online at http://chem.scichina.com and http://link.springer.com/journal/11426. The supporting materials are published as submitted, without typesetting or editing. The responsibility for scientific accuracy and content remains entirely with the authors.

1 Li Y. *Acc Chem Res*, 2012, 45: 723–733
2 Lin Y, Li Y, Zhan X. *Chem Soc Rev*, 2012, 41: 4245–4272
3 Lu L, Zheng T, Wu Q, Schneider AM, Zhao D, Yu L. *Chem Rev*, 2015, 115: 12666–12731
4 Anthony JE, Facchetti A, Heeney M, Marder SR, Zhan X. *Adv Mater*, 2010, 22: 3876–3892

5 Lin Y, Zhan X. *Mater Horiz*, 2014, 1: 470–488
6 Lin Y, Zhao F, He Q, Huo L, Wu Y, Parker TC, Ma W, Sun Y, Wang C, Zhu D, Heeger AJ, Marder SR, Zhan X. *J Am Chem Soc*, 2016, 138: 4955–4961
7 Zhong Y, Trinh MT, Chen R, Purdum GE, Khlyabich PP, Sezen M, Oh S, Zhu H, Fowler B, Zhang B, Wang W, Nam CY, Sfeir MY, Black CT, Steigerwald ML, Loo YL, Ng F, Zhu XY, Nuckolls C. *Nat Commun*, 2015, 6: 8242
8 Lin Y, He Q, Zhao F, Huo L, Mai J, Lu X, Su CJ, Li T, Wang J, Zhu J, Sun Y, Wang C, Zhan X. *J Am Chem Soc*, 2016, 138: 2973–2976
9 Hwang YJ, Li H, Courtright BAE, Subramaniyan S, Jenekhe SA. *Adv Mater*, 2016, 28: 124–131
10 Hwang YJ, Courtright BAE, Ferreira AS, Tolbert SH, Jenekhe SA. *Adv Mater*, 2015, 27: 4578–4584
11 Sun D, Meng D, Cai Y, Fan B, Li Y, Jiang W, Huo L, Sun Y, Wang Z. *J Am Chem Soc*, 2015, 137: 11156–11162
12 Gao L, Zhang ZG, Xue L, Min J, Zhang J, Wei Z, Li Y. *Adv Mater*, 2016, 28: 1884–1890
13 Meng D, Sun D, Zhong C, Liu T, Fan B, Huo L, Li Y, Jiang W, Choi H, Kim T, Kim JY, Sun Y, Wang Z, Heeger AJ. *J Am Chem Soc*, 2016, 138: 375–380
14 Lin H, Chen S, Li Z, Lai JYL, Yang G, McAfee T, Jiang K, Li Y, Liu Y, Hu H, Zhao J, Ma W, Ade H, Yan H. *Adv Mater*, 2015, 27: 7299–7304
15 Kwon OK, Uddin MA, Park JH, Park SK, Nguyen TL, Woo HY, Park SY. *Adv Mater*, 2016, 28: 910–916
16 Nielsen CB, Holliday S, Chen HY, Cryer SJ, McCulloch I. *Acc Chem Res*, 2015, 48: 2803–2812
17 Zhao W, Qian D, Zhang S, Li S, Inganäs O, Gao F, Hou J. *Adv Mater*, 2016, 28: 4734–4739
18 Bin H, Zhang ZG, Gao L, Chen S, Zhong L, Xue L, Yang C, Li Y. *J Am Chem Soc*, 2016, 138: 4657–4664
19 Cnops K, Zango G, Genoe J, Heremans P, Martinez-Diaz MV, Torres T, Cheyns D. *J Am Chem Soc*, 2015, 137: 8991–8997
20 Zhan X, Tan Z, Domercq B, An Z, Zhang X, Barlow S, Li Y, Zhu D, Kippelen B, Marder SR. *J Am Chem Soc*, 2007, 129: 7246–7247
21 Jung JW, Jo JW, Chueh CC, Liu F, Jo WH, Russell TP, Jen AKY. *Adv Mater*, 2015, 27: 3310–3317
22 Pho TV, Toma FM, Chabinyc ML, Wudl F. *Angew Chem Int Ed*, 2013, 52: 1446–1451
23 Cnops K, Rand BP, Cheyns D, Verreet B, Empl MA, Heremans P. *Nat Commun*, 2014, 5: 3406
24 Mu C, Liu P, Ma W, Jiang K, Zhao J, Zhang K, Chen Z, Wei Z, Yi Y, Wang J, Yang S, Huang F, Facchetti A, Ade H, Yan H. *Adv Mater*, 2014, 26: 7224–7230
25 Hartnett PE, Timalsina A, Matte HSSR, Zhou N, Guo X, Zhao W, Facchetti A, Chang RPH, Hersam MC, Wasielewski MR, Marks TJ. *J Am Chem Soc*, 2014, 136: 16345–16356
26 Diao Y, Zhou Y, Kurosawa T, Shaw L, Wang C, Park S, Guo Y, Reinspach JA, Gu K, Gu X, Tee BCK, Pang C, Yan H, Zhao D, Toney MF, Mannsfeld SCB, Bao Z. *Nat Commun*, 2015, 6: 7955
27 Holliday S, Ashraf RS, Nielsen CB, Kirkus M, Röhr JA, Tan CH, Collado-Fregoso E, Knall AC, Durrant JR, Nelson J, McCulloch I. *J Am Chem Soc*, 2015, 137: 898–904
28 Lin Y, Zhan X. *Acc Chem Res*, 2016, 49: 175–183
29 Lin Y, Zhang ZG, Bai H, Wang J, Yao Y, Li Y, Zhu D, Zhan X. *Energ Environ Sci*, 2015, 8: 610–616
30 Lin Y, Wang J, Zhang ZG, Bai H, Li Y, Zhu D, Zhan X. *Adv Mater*, 2015, 27: 1170–1174
31 Wu Y, Bai H, Wang Z, Cheng P, Zhu S, Wang Y, Ma W, Zhan X. *Energ Environ Sci*, 2015, 8: 3215–3221
32 Bai H, Wang Y, Cheng P, Wang J, Wu Y, Hou J, Zhan X. *J Mater Chem A*, 2015, 3: 1910–1914
33 Lin Y, Zhan X. *Adv Energ Mater*, 2015, 5: 1501063
34 Lin Y, Li T, Zhao F, Han L, Wang Z, Wu Y, He Q, Wang J, Huo L, Sun Y, Wang C, Ma W, Zhan X. *Adv Energ Mater*, 2016, 6: 1600854
35 Liao SH, Jhuo HJ, Cheng YS, Chen SA. *Adv Mater*, 2013, 25: 4766–4771
36 Lu X, Hlaing H, Nam CY, Yager KG, Black CT, Ocko BM. *Chem Mater*, 2015, 27: 60–66
37 Lu X, Hlaing H, Germack DS, Peet J, Jo WH, Andrienko D, Kremer K, Ocko BM. *Nat Commun*, 2012, 3: 795
38 Liao HC, Tsao CS, Shao YT, Chang SY, Huang YC, Chuang CM, Lin TH, Chen CY, Su CJ, Jeng US, Chen YF, Su WF. *Energ Environ Sci*, 2013, 6: 1938
39 Mai J, Lau TK, Xiao T, Su CJ, Jeng U, Zhao N, Xiao X, Lu X. *RSC Adv*, 2015, 5: 88500–88507